

MISSIONGNN: Hierarchical Multimodal GNN-based Weakly Supervised Video Anomaly Recognition with Mission-Specific Knowledge Graph Generation

Sanggeon Yun¹, Ryozo Masukawa¹, Minhyoung Na², and Mohsen Imani^{1,†}

¹University of California, Irvine

²Kookmin University

[†]Corresponding author, email: m.imani@uci.edu

Abstract—In the context of escalating safety concerns across various domains, the tasks of Video Anomaly Detection (VAD) and Video Anomaly Recognition (VAR) have emerged as critically important for applications in intelligent surveillance, evidence investigation, violence alerting, etc. These tasks, aimed at identifying and classifying deviations from normal behavior in video data, face significant challenges due to the rarity of anomalies which leads to extremely imbalanced data and the impracticality of extensive frame-level data annotation for supervised learning. This paper introduces a novel hierarchical graph neural network (GNN) based model MISSIONGNN that addresses these challenges by leveraging a state-of-the-art large language model and a comprehensive knowledge graph for efficient weakly supervised learning in VAR. Our approach circumvents the limitations of previous methods by avoiding heavy gradient computations on large multimodal models and enabling fully frame-level training without fixed video segmentation. Utilizing automated, mission-specific knowledge graph generation, our model provides a practical and efficient solution for real-time video analysis without the constraints of previous segmentation-based or multimodal approaches. Experimental validation on benchmark datasets demonstrates our model’s performance in VAD and VAR, highlighting its potential to redefine the landscape of anomaly detection and recognition in video surveillance systems.

I. INTRODUCTION

The escalating concern for safety across various sectors has heightened the importance of tasks like Video Anomaly Detection (VAD) and Video Anomaly Recognition (VAR). These tasks are crucial for applications such as intelligent surveillance [3], [7], evidence investigation [24], and violence alerting [13], [30], where the goal is to automatically identify and classify activities that deviate from normal patterns in video data [35]. VAD and VAR can potentially be approached through supervised learning to detect anomalies [2], [42]; however, the rarity of such anomalies leads to highly imbalanced datasets, complicating the training process. Moreover, the extensive effort and cost required for frame-level video data annotation render supervised learning with frame-level annotations impractical. Consequently, many researchers have shifted their focus towards weakly-supervised learning [17],

[36], [38], [48], [53], [60], which relies on video-level annotations to train models. This shift addresses the challenges posed by data imbalance and annotation costs but introduces new complexities in achieving accurate frame-level anomaly detection and recognition.

Recent advancements in tackling these challenges involve the use of pre-trained models to leverage the rich, embedded information they offer, thereby enhancing the distinction between normal and abnormal frames [28], [36], [44], [53], [60]. However, for VAR, the intricacies go beyond what pre-trained vision models can discern, necessitating finer granularity. To address this, some studies [28], [43], [44], [50], [53] have explored large multimodal neural networks [29], [31] capable of extracting more nuanced distributions, employing methods like learnable prompts [59] or adapters [44] to refine model differentiation. This approach, while innovative, demands substantial computational resources due to the gradient flow through these large models [12]. Furthermore, it is incompatible with the prevailing trend towards large pre-trained models, which are typically accessed via APIs, making it impossible to compute gradients directly.

Moreover, the application of multiple-instance learning (MIL) with fixed video segmentation has been a popular simplified strategy among researchers [36]. By dividing videos into fixed-size or fixed-number segments and introducing a transformer model to capture not only short-term relationships but also long-term relationships between segments, these models have shown improved performance [17], [38], [44], [48], [53], [57]. Yet, this method struggles with the variability of anomaly event durations e.g., events that happen in very short periods or video length is much longer than the event length, and the practical limitations of real-time analysis, where future frame data is unavailable, and past frame data is potentially infinite. Such reliance on long-term relationship modeling further complicates the deployment of these models in real-world scenarios, where rapid and continuous analysis is essential.

This paper proposes a novel approach MISSIONGNN to

tackle VAR by introducing a novel hierarchical graph neural network (GNN) based model that avoids the computational burdens associated with gradient computation of large multimodal models and introduces a fully frame-level training methodology without using MIL. Unlike prior work that limitedly utilized GNNs for temporal information processing [39], [57], our model uses GNN to capture semantic information using a mission-specific knowledge graph (KG) that is automatically generated by our KG generation framework using a large language model namely GPT-4 [1], and a large knowledge graph namely ConceptNet [34]. Instead of flowing gradient to a large multimodal model, our approach utilizes a built mission-specific knowledge graph and only uses the large multimodal model without any gradient computation to have initial embeddings for each node that will be used in our GNN. After that, our approach uses a small transformer to capture only short-term relationships. This innovative strategy enables effective anomaly detection without the need for gradient computations on large models, relying instead on light models while offering a practical, efficient, and scalable solution to the challenges of weakly-supervised learning in video anomaly recognition.

In summary, our work represents a fundamentally novel contribution to the field, offering the following key advancements:

- To the best of our knowledge, we propose MISIONGNN a novel hierarchical GNN-based model with an automated mission-specific knowledge graph generation framework to have an efficient weakly supervised video anomaly recognition model. Through our proposed mission-specific knowledge graph generation framework, our approach can be adopted in various other tasks.
- Unlike previous works on using pre-trained large multimodal models, our approach does not require heavy gradient computation on the pre-trained large multimodal models providing efficient training. At the same time, our approach provides additional flexibility that also can be implemented using large pre-trained models that are exclusively accessible through APIs which we do not have access to the weights of the model.
- Inspired by human intuition, we introduce completely frame-level training and inference that does not require video segmentation which can affect the model’s performance by merging multiple frames into fixed-size segments. Furthermore, this makes our model more practical in real applications by not using future segments or past segments.

II. RELATED WORKS

A. Weakly Supervised Video Anomaly Detection and Recognition

The study of anomaly detection in videos has evolved significantly, beginning with methods that heavily relied on fully supervised techniques [2], [42] requiring detailed frame-by-frame labels. To overcome the challenges and high costs

associated with detailed annotations, researchers have shifted towards using less resource-intensive approaches. These include weakly supervised methods that train models [17], [36], [38], [48] with broader video-level labels, one-class classification techniques [21], [23], [27] focusing only on normal data, and unsupervised strategies [25], [52] that operate without any labels. Among these, weakly supervised methods have shown notable promise, offering a balance between performance and annotation costs. Our approach aligns with this trend, adopting weakly supervised learning to advance research in this area.

The concept of multiple-instance learning [36] which is dividing videos into segments or bags and treating all frames within a segment as having the same label has become a foundational technique in weakly supervised video anomaly detection. This method, along with enhancements such as internal loss constraints within bags [55] and refinements in segment-level pseudo labeling [57], has facilitated the development of temporal models [17], [38], [39], [44], [48], [53], [57] capable of understanding both short and long-term segment relationships. Unlike these methods, our research seeks new directions beyond the MIL framework to address its limitations, especially in handling variable anomaly durations and the need for real-time analysis which previous works have impracticality in terms of real-time analysis scenarios caused by relying on long-term relationships.

While VAD has received considerable attention, VAR remains underexplored with only a few works focused on it [53], primarily due to the scarcity of samples for each type of anomaly [36]. This scarcity makes VAR a more daunting task than related fields like action recognition [20], [26], [32]. Notably, from the previous work [53], several previous models [17], [38], [47] showed performance drops on some benchmark datasets when it comes to VAR using the mean area under the curve (mAUC) score which is the mean score of the area under the curve (AUC) scores for each anomaly type. However, as Large Language and Vision (LLV) models [29], [31] are introduced to solve action recognition tasks showing success in improving recognition performance [43], [50], an effort to utilize such LLV in VAR tasks is also attempted [53], [54]. These works showed that using LLV that can extract richer features learned from a large dataset of image-caption pairs can enable enhanced anomaly recognition. Our work introduces an innovative way to adapt large multimodality models to tackle the challenges of VAR in a weakly supervised manner.

B. Graph Neural Networks and Knowledge Graphs

Graph Neural Networks, including Graph Convolution Networks (GCNs) [56] and Graph Attention Networks (GATs) [41], have been pivotal in processing structural information represented as nodes and edges. The Message Passing Network framework [10] exemplifies a generalized model for GNNs. The network consists of three functions: message function, aggregate function, and update function. Each function can be implemented using simple neural networks with nonlinear functions. Using the message function, it computes

messages for all edges and then, each node aggregates messages from neighboring nodes. The aggregation can be sum, mean, or other functions. Finally, it uses the update function to have embeddings of each node from given aggregations. These processes facilitate the generation of node embeddings that capture the essence of the graph's structure.

GNNs are frequently paired with knowledge graphs to address a wide array of tasks, from question answering [51] and information retrieval [8] to reasoning [9]. Utilizing large-scale, general-domain knowledge graphs like ConceptNet [34], which is one of the widely used semantic knowledge graphs that contain different types of relationships between words, researchers can construct detailed knowledge graphs that enhance model understanding and reasoning capabilities [4], [33], [45]. In our work, we also use ConceptNet in our automated knowledge graph generation framework as one of the structured knowledge sources.

Although a few previous works [39], [57] used GNN as a part of their methods for VAD tasks, their usage of GNN models was limited in capturing temporal relationships between pairs of frames. In contrast, we use a novel GNN architecture over a knowledge graph constructed from our automated knowledge graph generation framework to do reasoning for the VAR task.

C. Large Multimodal Models and Prompt Optimization

After a huge success in large language models [5], [6], [46], new approaches to have multimodal neural networks [29], [31], which not only can process text but also other forms of modality such as images, emerged. Early models trained to learn joint visual-text embedding spaces with the help of caption-image pairs which are called Large Language and Vision models that can embed given images and text in the same embedding space. LLV models are implemented by having modality-specific encoders and trained with contrastive learning techniques on diverse datasets to align the data representations from different modalities [14], [29]. These LLV models are effective in capturing reacher highly generalized embeddings enabling extension to detection or recognition tasks on images or videos [44], [50], [53] mainly utilizing CLIP [29]. Among those, AnomalyCLIP [53] proposed a model utilizing CLIP to solve the VAR problem demonstrating the strengths of leveraging large multimodal models on VAR tasks by achieving higher mAUC compared to the previous methods. Recently, large multimodal models that can support an expanded range of modalities compared to LLV have been proposed such as ImageBind [11] which can support six different modalities. Our work extends this progress by incorporating ImageBind aiming to explore new possibilities in multimodal anomaly detection although it has similar encoder models with CLIP for text and images.

Prompt optimization techniques have emerged to have better embedding representations to improve models' performance. Early works conducted human-engineered prompts which manually craft more optimal prompts [15]. Later, to resolve the impracticality of the manual prompting, learnable prompt

methods that learn optimal prompt tokens' embedding using gradients of large multimodal models were introduced [16], [18]. Despite its potential, the learnable prompt approach caused easy overfitting issues [58] with its inefficiency in computing the large model's gradient hindering its scalability, which makes the approach impractical [61]. Our research proposes an alternative strategy, replacing prompt optimization with knowledge graph reasoning to bypass the limitations of prompt optimization, offering a fresh perspective on enhancing model efficacy.

III. METHODOLOGY

A. Overall Pipeline

Our proposed approach consists of two major frameworks: mission-specific knowledge graph generation and hierarchical graph neural network-based detection. First, the mission-specific KG generation framework is used for generating KG that can extract useful information from a given frame image. In VAR, each mission-specific KG indicates a KG that contains structured knowledge regarding the corresponding anomaly type. Through this automated framework, our method builds n mission-specific KG each corresponding to one of the n anomaly types. The generated mission-specific KGs are used in the following framework, hierarchical GNN-based detection. n hierarchical GNNs are paired with one of the n mission-specific KGs to conduct reasoning over the extracted knowledge to conduct the corresponding mission which is detecting a certain type of anomaly. And large multimodal model's embedding of each frame is processed by each of the GNN models. Now, embeddings from the final embedding node of each GNN model are concatenated into a single embedding vector that represents reasoning results from all mission-specific KGs. The final vector now is conveyed to a short-term temporal model with the previous consecutive 29 frames. Note that this temporal model only considers short-term relationships which does not require long frame sequence as an input. The resulting output from the short-term temporal model passes through a final decision model to have a final score distribution for each anomaly.

Details are discussed in the following subsections: we first address our mission-specific KG generation framework in subsection III-B, then the proposed hierarchical multimodal GNN model and short-term temporal model are introduced in subsection III-C and subsection III-D respectively, and finally training losses are described in subsection III-E.

B. Mission-Specific Knowledge Graph Generation Framework

Figure 1 shows the overall framework for mission-specific knowledge graph generation. Given a mission m_i from a user, the framework generates a KG $G_{m_i} = (V_{m_i}, E_{m_i})$, which is directed acyclic graph (DAG). In order to generate G_{m_i} , it first, combines the given mission m_i with a pre-formatted prompt to have a query message. Then, n_{cpt} number of key concept words $w_{m_i,j}^{cpt}$ are extracted by querying the generated query message to a large language model. Each word $w_{m_i,j}^{cpt}$ is considered as a key concept node $v_{m_i,j}^{cpt}$ and those key concept

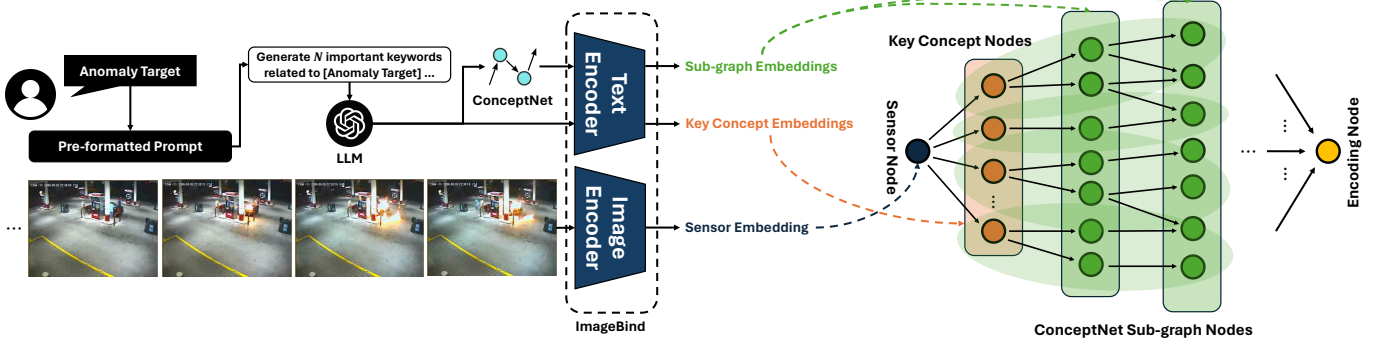


Fig. 1. The framework for mission-specific knowledge graph generation.

nodes build part of the KG $\{v_{m_i,j}^{cpt}\} = V_{m_i}^{cpt} \subset V_{m_i}$. Next, to expand KG, iterative sub-graph extraction is conducted using ConceptNet. First sub-graph nodes $v_{m_i,j}^{sub_1} \in V_{m_i}^{sub_1}$ are retrieved from ConceptNet which are directly neighboring to $v_{m_i,j}^{cpt} \in V_{m_i}^{cpt}$. A set of edges containing neighboring relationships $E_{m_i}^{sub_1} = \{(v, u) \in V_{m_i}^{cpt} \times V_{m_i}^{sub_1} \mid (v, u) \in \text{ConceptNet}\}$ is also extracted during the process. In our implementation, we only considered the “/r/RelatedTo” relationship type. Next sub-graph nodes $v_{m_i,j}^{sub_2} \in V_{m_i}^{sub_2}$ are extracted with the similar way but directly neighboring to $V_{m_i}^{sub_1}$ with edges $E_{m_i}^{sub_2} = \{(v, u) \in V_{m_i}^{sub_1} \times V_{m_i}^{sub_2} \mid (v, u) \in \text{ConceptNet}\}$. This process, which is extracting $k + 1^{th}$ set of sub-graph nodes $V_{m_i}^{sub_{k+1}}$ and edges $E_{m_i}^{sub_{k+1}}$ from $V_{m_i}^{sub_k}$, is iteratively conducted until $V_{m_i}^{sub_{d_{sub}}}$ and $E_{m_i}^{sub_{d_{sub}}}$ are retrieved where d_{sub} indicates maximum depth of the sub-graph. The extracted sub-graph nodes $V_{m_i}^{sub} = \bigcup_{1 \leq k \leq d_{sub}} V_{m_i}^{sub_k}$ and edges $E_{m_i}^{sub} = \bigcup_{1 \leq k \leq d_{sub}} E_{m_i}^{sub_k}$ also build part of the KG by $V_{m_i}^{sub} \subset V_{m_i}$ and $E_{m_i}^{sub} \subset E_{m_i}$. Finally, G_{m_i} is completed by combining sensor node $v_{m_i}^{snr}$ and encoding node $v_{m_i}^{ecd}$. $v_{m_i}^{snr}$ is attached to the graph by connecting it with key concept nodes $v_{m_i,j}^{cpt}$ towards $v_{m_i,j}^{cpt}$ direction while $v_{m_i}^{ecd}$ is attached by connecting it with leaf nodes, which are nodes that do not have outgoing edges, of sub-graph nodes towards $v_{m_i}^{ecd}$ direction. Completed G_{m_i} is described in Equation 1.

$$\begin{aligned}
 V_{m_i} &= \{v_{m_i}^{snr}\} \cup V_{m_i}^{cpt} \cup V_{m_i}^{sub} \cup \{v_{m_i}^{ecd}\} \\
 E_{m_i} &= \{(v_{m_i}^{snr}, u) \mid u \in V_{m_i}^{cpt}\} \\
 &\cup E_{m_i}^{sub} \\
 &\cup \{(v, v_{m_i}^{ecd}) \mid v \in V_{m_i}^{sub} \wedge (v, u) \notin E_{m_i}^{sub} \forall u \in V_{m_i}^{sub}\}
 \end{aligned} \tag{1}$$

To process generated KG G_{m_i} using GNN later, it is necessary to have embeddings of the nodes. For having embedding representations, we use text encoder $\mathcal{E}_T(\cdot)$ for embedding key concept nodes and sub-graph nodes and image encoder $\mathcal{E}_I(\cdot)$ for embedding the sensor node. By using encoders $\mathcal{E}_T(\cdot)$ and $\mathcal{E}_I(\cdot)$ from the pre-trained ImageBind model, we can have embeddings in the same embedding space for different modalities. For the encoding node, it is initialized with a 0 valued vector. In VAR, multiple mission-specific KGs G_{m_i}

are generated by setting each mission m_i as detecting each anomaly type T_i . As a result, for the VAR task of n number of anomaly types, a total of n mission-specific KGs G_{T_i} are built by the framework.

C. Hierarchical Multimodal GNN

For a given frame image F_t and mission-specific KGs G_{T_i} , to conduct reasoning for each KG, our proposed hierarchical multimodal GNN model is used over each given KG as presented in Figure 2. For each KG G_{T_i} , the reasoning process propagates from a sensor node of G_{T_i} to its embedding node. To conduct the reasoning process, first, a given frame image F_t is encoded by $\mathcal{E}_I(F_t)$ and used as an embedding vector of the sensor node $v_{m_i}^{snr}$. Next, $d_{sub} + 2$ GNN layers are applied hierarchical way so that reasoning by GNN layers can propagate starting from the sensor node and the final resulting embedding can be located in the embedding node. Each GNN layer $\mathcal{G}_{m_i,l}(\cdot)$ consists of 5 sub-layers: dense layer, hierarchical message passing layer, hierarchical aggregate layer, batch normalization layer, and activation layer. Dense layer $\phi_{m_i,l}: \mathbb{R}^{|V_{m_i}| \times D_{l-1}} \rightarrow \mathbb{R}^{|V_{m_i}| \times D_l}$, where $D_{m_i,l-1}$ indicates dimensionality of previous layer and $D_{m_i,l}$ indicates dimensionality of the current layer, transfers embedding space to have better relationship representations between each knowledge edge embedding and can be formulated as follows:

$$\phi_{m_i,l}(X_{l-1}) = \mathbf{W}_{m_i,l}^\phi X_{l-1} + \mathbf{b}_{m_i,l}^\phi \tag{2}$$

where $\mathbf{W}_{m_i,l}^\phi$ is trainable parametric matrix, $\mathbf{b}_{m_i,l}^\phi$ is trainable bias, and $X_{l-1} \in \mathbb{R}^{|V_{m_i}| \times D_{m_i,l-1}}$ is embeddings of previous layer for nodes. Hierarchical message passing layer $\mathcal{M}_{m_i,l}^h: \mathbb{R}^{|V_{m_i}| \times D_{m_i,l}} \rightarrow \mathbb{R}^{|E_{m_i}^{(l)}| \times D_{m_i,l}}$ compute messages each corresponding to each node where $E_{m_i}^{(l)} \subset E_{m_i}$ indicates a set of edges that connect depth $l - 1$ nodes $V_{m_i}^{(l-1)} \subset V_{m_i}$ and depth l nodes $V_{m_i}^{(l)} \subset V_{m_i}$. Note that depth 0 node set $V_{m_i}^{(0)}$ contains only one node which is sensor node $v_{m_i}^{snr}$ and l starts from 1. Each message indicates measured relativity by the dot product between two knowledge embeddings as described below:

$$\mathcal{M}_{m_i,l}^h(X) = \{X_s \cdot X_d\}_{(s,d) \in E_{m_i}^{(l)}} \tag{3}$$

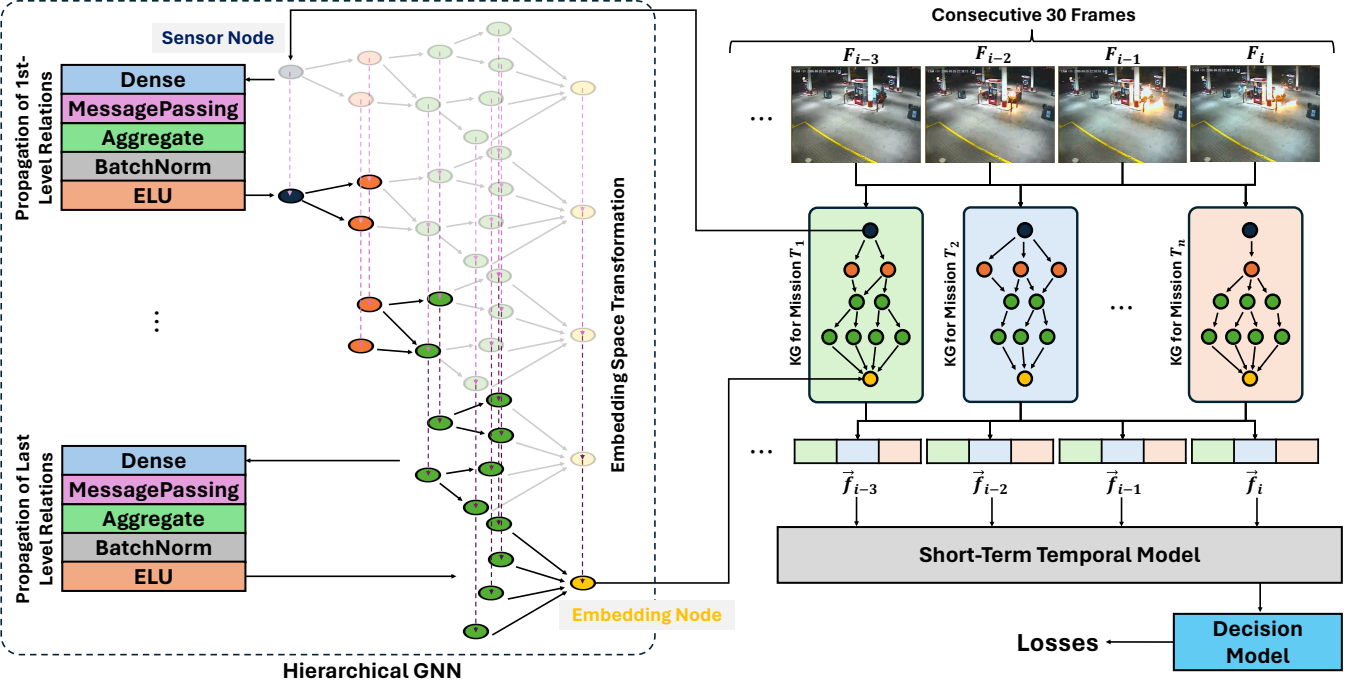


Fig. 2. The overall framework for our proposed model utilizing the novel concept of hierarchical graph neural network.

where s indicates source node, d indicates destination node, and $X \in \mathbb{R}^{|V_{m_i}| \times D_{m_i,l}}$ is node embeddings. Hierarchical aggregate layer $\mathcal{A}_{m_i,l}^h: \{\mathbb{R}^{|V_{m_i}| \times D_{m_i,l}}, \mathbb{R}^{|E_{m_i}^{(l)}| \times D_{m_i,l}}\} \rightarrow \mathbb{R}^{|V_{m_i}| \times D_{m_i,l}}$ aggregates all the passed messages from source nodes into a single vector by getting a mean vector meanwhile remaining other embeddings of nodes that do not have messages from their source nodes, denoted as:

$$\mathcal{A}_{m_i,l}^h(X, M) = \left\{ X_d \mathbf{1}(d \notin V_{m_i}^{(l)}) + \frac{\sum_{(s,d) \in E_{m_i}^{(l)}} M_{s,d}}{|\{s \in V_{m_i} | (s,d) \in E_{m_i}^{(l)}\}|} \mathbf{1}(d \in V_{m_i}^{(l)}) \right\}_{d \in V_{m_i}}$$
(4)

where $X \in \mathbb{R}^{|V_{m_i}| \times D_{m_i,l}}$ indicates node embeddings, $M \in \mathbb{R}^{|E_{m_i}^{(l)}| \times D_{m_i,l}}$ indicates messages from $\mathcal{A}_{m_i,l}^h$, and $\mathbf{1}(\cdot)$ indicates a function that gives 1 if a given statement is true otherwise 0. The final form of the GNN layer at layer l is formulated as follows:

$$\begin{aligned} \mathcal{G}_{m_i,l}(X_{l-1}) = \\ \text{ELU}(\text{BatchNorm}(\mathcal{A}_{m_i,l}^h(\phi_{m_i,l}(X_{l-1}), M_{m_i,l}^h(\phi_{m_i,l}(X_{l-1})))) \end{aligned} \quad (5)$$

through this, knowledge embeddings of the current layer are computed $X_l = \mathcal{G}_{m_i,l}(X_{l-1}) \in \mathbb{R}^{|V_{m_i}| \times D_{m_i,l}}$ from previous layer embeddings $X_{l-1} \in \mathbb{R}^{|V_{m_i}| \times D_{m_i,l-1}}$. It is notable that unlike $\mathcal{M}_{m_i,l}^h$ and $\mathcal{A}_{m_i,l}^h$ where it is conducted only for $V_{m_i}^{(l)}$ nodes and $E_{m_i}^{(l)}$ edges, other components are applied for all nodes V_{m_i} and edges E_{m_i} so that embeddings of every node can be placed in the same embedding space for the future reasoning propagation. The final embedding of the

KG reasoning \vec{r}_{T_i} is extracted from $v_{m_i}^{ecd}$ of $X_{d_{sub}+2}$ which is the final embedding layer of KG G_{T_i} . Finally, reasoning embedding \vec{f}_t of the frame image encoding $\mathcal{E}_I(F_t)$ is formed by concatenating all \vec{r}_{T_i} from each KG as $\vec{f}_t = \vec{r}_{T_1} \frown \vec{r}_{T_2} \frown \dots \frown \vec{r}_{T_n} \in \mathbb{R}^D$ where $D = \sum_i D_{m_i,d_{sub}+2}$.

D. Short-term Temporal Model

Using multiple KGs and reasoning over them with our proposed hierarchical GNNs only considers information from a single frame. To extract richer information by exploiting video data, we use transformer-based temporal model $\mathcal{T}: \mathbb{R}^{T \times D} \rightarrow \mathbb{R}^D$ where T indicates the number of consecutive frames. Specifically, we use simple a single transformer encoder layer [40] and put a sequence of reasoning embeddings including reasoning embeddings of previous $T-1$ consecutive frames $\vec{F}_t = \{\vec{f}_{t-T+1}, \vec{f}_{t-T+2}, \dots, \vec{f}_t\} \in \mathbb{R}^{T \times D}$ to the transformer and only takes the last output embedding $\vec{f}_t' = \mathcal{T}(\vec{F}_t) \in \mathbb{R}^D$ which is corresponding to the last input \vec{f}_t . This process is also presented in Figure 2. Unlike previous methods that considered not only short-term temporal relationships but also long-term temporal relationships, our model focuses on short-term relationships only by setting $T = 30$ without any video segmentation. In VAR, we assume that anomalies occur in short time intervals by following human intuition, i.e. when people encounter anomalies such as gunshots, they can detect them immediately without having to understand long-term relationships. The output of the short-term temporal model \vec{f}_t' is then processed by a decision model $f^{dec}: \mathbb{R}^D \rightarrow \mathbb{R}^{n+1}$ which is consists of a simple linear layer

and softmax function:

$$f^{dec}(\vec{f}_t) = \text{Softmax}(\mathbf{W}^{dec} \vec{f}_t + \mathbf{b}^{dec}) \quad (6)$$

where \mathbf{W}^{dec} is trainable parametric matrix, and \mathbf{b}^{dec} is trainable bias. The output of the decision model $\vec{s}_t = f^{dec}(\vec{f}_t)$ contains the estimated probability of the given frame F_t is normal $p_N(F_t) = \vec{s}_{t,0}$ and probabilities of the frame belong to each anomaly type $i \in \{1, 2, \dots, n\}$: $p_{A,i}(F_t) = p_A(F_t)p_{i|A}(F_t) = \vec{s}_{t,i}$ where $p_A(F_t) = 1 - p_N(F_t)$ indicates probability of abnormal and $p_{i|A}(F_t) = \frac{\vec{s}_{t,i}}{1 - p_N(F_t)}$ indicates conditional probability of anomaly type i when it is anomaly.

E. Weakly-supervised Frame-level Training

1) *Decaying Threshold-based Anomaly Localization*.: A better performing model requires estimating normal frames and anomaly frames among frames in the same video, where a single type of anomaly is labeled in weakly-supervised learning. However, it is difficult to implement a widely used rank-based approach without using MIL-based training. To resolve this issue and have a model that is capable of fully frame-level training and inference, we introduce a novel anomaly localization method, which is a method that separates normal frames from anomaly-labeled video, using our proposed concept of decaying threshold. Decaying threshold θ_d is denoted as follows:

$$\theta_d^{(iter)} = \frac{\theta_0 \alpha_d^{iter}}{2} + 0.5 \quad (7)$$

where θ_0 indicates initial value of θ_d , α_d indicates threshold decay rate, and $iter$ indicates current iteration of training. For each training iteration $iter$, frames F_t from anomaly-labeled videos are considered as normal frames when $p_A(F_t) = 1 - p_N(F_t) \leq 1 - \theta_d^{(iter)}$ is satisfied. In our implementation, we set $\theta_0 = 1$ so that the model initially considers every frame in anomaly-labeled videos as an anomaly frame and slowly approaches 0.5 as it separates normal frames. We assume that while all reasoning embeddings of frames F_t^A from anomaly-labeled videos separated from reasoning embeddings of frames F_t^N from normal-labeled videos, the ones F_t^{A+} that are similar to normal-labeled frames ($p_A(F_t^{A+}) \leq 1 - \theta_d^{(iter)}$) slowly separated from the anomaly distribution, which makes them be separated later from anomaly distribution F_t^{A-} that separated faster ($p_A(F_t^{A-}) > 1 - \theta_d^{(iter)}$) by the decaying threshold.

2) *Cross-entropy Loss*.: After the decaying threshold-based anomaly localization, we have normal frames F_t^N , normal estimated frames F_t^{A+} , and anomaly estimated frames F_t^{A-} . We use the cross-entropy loss to maximize probabilities that match each case. Thus, we have three cross-entropy terms for each set of cases as follows:

$$\mathcal{L}_N = -\frac{\lambda_N}{|F^N|} \sum_t \log p_N(F_t^N) \quad (8)$$

$$\mathcal{L}_{A+} = -\frac{\lambda_N}{|F^{A+}|} \sum_t \log p_N(F_t^{A+}) \quad (9)$$

$$\mathcal{L}_{A-} = -\frac{1}{|F^{A-}|} \sum_t \lambda_{A,y_t} \log p_{A,y_t}(F_t^{A-}) \quad (10)$$

where y_t indicates the corresponding anomaly type, λ_N indicates loss weight for normal cross-entropy, and $\lambda_{A,c}$ indicates loss weight for anomaly class c cross-entropy. λ_N and $\lambda_{A,c}$ are adjusted to cope with data imbalance.

3) *Sparsity and Smoothing Losses*.: We adapted the same two regularization loss terms that are used in [37]. First is done through sparsity loss term exploiting that the anomaly cases are rare in entire time frames. Sparsity loss tries to minimize the number of frames that are predicted as anomalies by following:

$$\mathcal{L}_{spa} = \frac{1}{|F^A|} \sum_t p_A(F_t^A) \quad (11)$$

Note that it is only applied to frames from anomaly-labeled videos. Also, to make predictions smoother along the time dimension, another loss term smoothing loss is implemented as follows:

$$\mathcal{L}_{smt} = \frac{1}{|F|} \sum_t (p_A(F_t) - p_A(F_{t-1}))^2 \quad (12)$$

where F_t and F_{t-1} are consecutive two frames.

By combining all loss terms, final loss \mathcal{L} is formed as follows:

$$\mathcal{L} = \mathcal{L}_N + \mathcal{L}_{A+} + \mathcal{L}_{A-} + \lambda_{spa} \mathcal{L}_{spa} + \lambda_{smt} \mathcal{L}_{smt} \quad (13)$$

where λ_{spa} and λ_{smt} indicate balance coefficients for sparsity loss and smoothing loss term respectively.

IV. EXPERIMENTS

A. Experimental Settings

1) *Implementation Details*.: For our multimodal embedding model, we use the pre-trained ImageBind huge model. Also, for the mission-specific KG generation, we use GPT-4 and ConceptNet 5. The loss term balance coefficients λ_{spa} and λ_{smt} are set to 0.001 for both of them. We utilize the AdamW [22] as the optimizer with learning rate of 10^{-5} , a weight decay of 1.0, $\beta_1 = 0.9$, $\beta_2 = 0.999$, and $\epsilon = 10^{-8}$. The decaying threshold α_d is set to 0.9999. For our GNN models, we set the dimensionality all the same $D_{m_i,l} = 8$. In the case of the short-term temporal model, we use an inner dimensionality of 128 with 8 attention heads. Finally, the model is trained for 3,000 steps with a mini-batch of 128.

2) *Evaluation Metrics*.: We perform evaluations that include both VAD and VAR. Consistent with previous research, VAD performance is measured using the area under the curve (AUC) of the receiver operating characteristics (ROC) at the frame level. This metric is chosen because it is independent of thresholding in the detection task. A higher AUC at the frame level indicates a better ability to distinguish normal from abnormal events. For the VAR evaluation, we extend the AUC metric to the multi-classification scenario. Specifically, we compute the AUC for each anomalous class, treating anomalous frames of the class as positive instances and all others as negative instances. We then compute the mean AUC (mAUC) across all anomalous classes. Likewise, for the XD-Violence dataset, we follow the established evaluation

protocol [49] and VAD results are presented using the average precision (AP) derived from the precision-recall curve (PRC). For VAR outcomes, we report the mean average precision (mAP), which involves averaging the binary AP values across all abnormal classes.

B. Datasets

Our experiments utilize two Video Anomaly Detection (VAD) datasets: UCF-Crime [37] and XD-Violence [49]. Additionally, the ShanghaiTech dataset [19], comprising 437 videos captured from diverse surveillance cameras on a university campus, is commonly employed in this research field. However, since some anomaly class labels are only present in the training dataset, we have determined that ShanghaiTech is not suitable for evaluating our method. Therefore, we have chosen not to include it in our evaluation process.

UCF-Crime is an extensive dataset comprising 1900 untrimmed surveillance videos depicting 13 real-world anomalies with significant implications for public safety. The training set comprises 800 normal and 810 anomalous videos, while the testing set includes the remaining 150 normal and 140 anomalous videos.

XD-Violence, a large-scale violence detection dataset, which consists of 4754 untrimmed videos with audio signals and weak labels. It is partitioned into a training set of 3954 videos and a test set of 800 videos, totaling 217 hours in duration and covering various scenarios with 6 anomaly categories. Notably, each violent video may carry multiple labels, ranging from 1 to 3. To align with our training setup, where only one anomaly type per video is considered, we curate a subset comprising 4463 videos containing at most one anomaly.

C. Evaluation on Training Memory Efficiency

To demonstrate the advantage in training in terms of memory consumption of our proposed approach, we measured GPU memory consumption specifically the amount of memory for computing computational graphs which is required to conduct gradient backpropagation. Table I shows measured GPU memory consumption used for computational graphs for each of ImageBind and our GNN model by different batch sizes. We can observe that our model consumes $2.66 \times$ to $5.45 \times$ lower memory. Considering previous approaches used learnable prompts or other types of gradient computation of the LLVs are also using additional models to process the output from the LLV, the memory efficiency can be increased. It enables memory-efficient training while maintaining or outperforming previous models in some benchmarks that are shown in subsection IV-D.

D. Evaluation on VAD and VAR

Table II and Table III show the evaluation results of both VAD and VAR tasks on UCF-Crime dataset and XD-Violence dataset respectively. MISSIONGNN surpasses the performance of cutting-edge VAR tasks in the UCF-Crime dataset, albeit showing a slight lag in VAD tasks. In contrast, AnomalyCLIP

exhibits superior performance in VAR tasks within the XD-Violence dataset, while our framework notably outperforms state-of-the-art VAD tasks in the same dataset.

V. DISCUSSION

Trade-off between VAD and VAR performance in different dataset settings. UCF-Crime dataset comprises videos recorded exclusively by fixed surveillance cameras in real-world settings, where the majority of video frames exhibit consistent backgrounds. In contrast, the XD-Violence dataset offers a diverse range of videos, spanning from movies to basketball games, resulting in frequent changes in camera position between frames. This variability poses a challenge to the ability of our proposed method to effectively capture short-term recognition. MISSIONGNN outperforms state-of-the-art VAR tasks in the UCF-Crime dataset but lags slightly behind in VAD tasks. Conversely, AnomalyCLIP [53] demonstrates superior performance in terms of VAR within the XD-Violence dataset, while our framework significantly outperforms state-of-the-art VAD tasks in the same dataset. AnomalyCLIP's advantage stems from its comprehensive analysis of all video frames, incorporating information from past to future by processing entire video snippets. However, training with future values can lead to overly optimistic results and may not be pragmatic for real-world deployment.

Inspired by human intuition, MISSIONGNN is constrained to classify 30 frames. The primary limitation of our proposed method lies in its inability to capture long-term dependencies for anomaly detection. However, in real-world applications such as violence alerting, timely responsiveness is crucial for effective anomaly detection. Therefore, there is a critical need for anomaly detection models with rapid response capabilities. Our proposed method achieves superior results compared to state-of-the-art models while meeting these requirements for both VAD and VAR, making a significant contribution to the field.

Limitations on mission-specific graph generation. Even though we introduce our GNN reasoning approach to deal with the heavy gradient computation from large pre-trained models, the efficacy of our framework heavily relies on the configuration of each mission-specific KG which can limit the performance of the model. Specifically, the construction of mission-specific KGs is facilitated by the output of GPT-4, which denotes the relevant terms associated with each mission. As a result, particularly in the context of VAR tasks, the selection of inappropriate terms by GPT-4 can significantly impair the model's performance even with our reasoning GNN model. In contrast, AnomalyCLIP adopts gradient-based prompt optimization, which is advantageous for more effective related word vector extraction at the cost of necessitating extensive gradient computations. Thus, there exists a trade-off between the computational cost of prompt optimization. Future efforts will focus on mitigating the trade-off relationship by addressing the constraints of our mission-specific graph generation framework. This study will aid in

TABLE I
MEMORY REQUIREMENTS FOR COMPUTATIONAL GRAPH OVER EACH MODEL IN MiB.

Batch Size	Model		Efficiency
	ImageBind	MISSIONGNN	
1	2,171	787	2.75×
32	5,240	960	5.45×
64	5,594	1,508	3.70×
128	5,948	2,228	2.66×

TABLE II
RESULTS OF THE STATE-OF-THE-ART METHODS AND MISSIONGNN ON UCF-CRIME

Method	Class												mAUC	AUC	
	Abuse	Arrest	Arson	Assault	Burglary	Explosion	Fighting	RoadAcc.	Robbery	Shooting	Shoplifting	Stealing	Vandalism		
RTFM [38]	79.99	62.57	90.53	82.27	85.53	92.76	85.21	90.31	81.17	82.82	92.56	90.23	87.20	84.86	84.03
S3R [47]	86.38	68.45	92.19	93.55	86.91	93.55	81.69	85.03	82.07	85.32	91.64	94.59	83.82	86.55	85.99
SSRL [17]	95.33	79.26	93.27	91.74	89.06	92.25	87.36	80.24	87.75	84.5	92.31	94.22	88.17	88.88	87.43
ActionCLIP [43]	91.88	90.47	89.21	86.87	81.31	94.08	83.23	94.34	82.82	70.53	91.60	94.06	89.89	87.71	82.30
AnomalyCLIP [53]	75.03	94.56	96.66	94.80	90.08	94.79	88.76	93.30	86.85	87.45	89.47	97.00	89.78	90.66	86.36
CLIP zero-shot [29]	57.37	80.65	91.72	80.83	74.34	90.31	83.54	87.46	70.22	63.99	71.21	45.49	66.45	74.12	58.63
MISSIONGNN (Ours)	93.68	87.64	94.15	95.86	92.31	94.73	89.44	97.16	81.40	90.57	92.94	97.74	81.77	91.49	84.48

TABLE III
RESULTS OF THE STATE-OF-THE-ART METHODS AND MISSIONGNN ON XD-VIOLENCE

Method	Class						mAP	AP
	Abuse	CarAccident	Explosion	Fighting	Riot	Shooting		
RTFM [38]	9.25	25.36	53.53	61.73	90.38	18.01	43.04	77.81
S3R [47]	2.63	23.82	45.29	49.88	90.41	4.34	36.06	80.26
ActionCLIP [43]	2.73	25.15	55.28	58.09	87.31	12.87	40.24	61.01
AnomalyCLIP [53]	6.10	31.31	68.75	71.44	92.74	26.13	49.41	78.51
CLIP zero-shot [29]	0.32	12.21	22.26	25.25	66.60	1.26	21.32	27.21
MISSIONGNN (Ours)	10.98	8.91	42.49	32.69	81.64	11.78	31.41	98.42

tackling the trend where many LLMs are accessible solely through APIs, hindering direct access to their model weights.

Limitations on anomaly localization. Given that our decaying threshold-based anomaly localization method shown in Equation 7. alters the threshold statically, without taking into account the distribution of video frames, it becomes imperative to meticulously select the hyperparameter α_d^{iter} to achieve satisfactory test outcomes. In future works, it is essential to devise a mechanism that eliminates the necessity of employing this hyperparameter and instead enables dynamic adjustment of the threshold during model training.

VI. CONCLUSIONS

In conclusion, our study introduces MISSIONGNN a novel hierarchical multimodal GNN-based approach for weakly-supervised video anomaly recognition, leveraging an automatically generated mission-specific knowledge graph to efficiently address the challenges of anomaly detection in video data. By circumventing the computational burdens from gradient computation of large multimodal models and eschewing fixed video segmentation, our model enables fully frame-level training and inference, demonstrating state-of-the-art performance on benchmark datasets while having training efficiency in terms of less GPU memory usage. This work not only marks a significant advancement in VAR but also offers a scalable,

practical framework applicable to a broad range of real-world scenarios, paving the way for future innovations in intelligent surveillance and beyond.

ACKNOWLEDGEMENTS

This work was supported in part by the DARPA Young Faculty Award, the National Science Foundation (NSF) under Grants #2127780, #2319198, #2321840, #2312517, and #2235472, the Semiconductor Research Corporation (SRC), the Office of Naval Research through the Young Investigator Program Award, and Grants #N00014-21-1-2225 and #N00014-22-1-2067. Additionally, support was provided by the Air Force Office of Scientific Research under Award #FA9550-22-1-0253, along with generous gifts from Xilinx and Cisco.

REFERENCES

- [1] J. Achiam, S. Adler, S. Agarwal, L. Ahmad, I. Akkaya, F. L. Aleman, D. Almeida, J. Altenschmidt, S. Altman, S. Anadkat *et al.*, “Gpt-4 technical report,” *arXiv preprint arXiv:2303.08774*, 2023.
- [2] S. Bai, Z. He, Y. Lei, W. Wu, C. Zhu, M. Sun, and J. Yan, “Traffic anomaly detection via perspective map based on spatial-temporal information matrix,” in *CVPR Workshops*, 2019, pp. 117–124.
- [3] Q. Bao, F. Liu, Y. Liu, L. Jiao, X. Liu, and L. Li, “Hierarchical scene normality-binding modeling for anomaly detection in surveillance videos,” in *Proceedings of the 30th ACM International Conference on Multimedia*, 2022, pp. 6103–6112.

[4] A. Bosselut, H. Rashkin, M. Sap, C. Malaviya, A. Celikyilmaz, and Y. Choi, “Comet: Commonsense transformers for automatic knowledge graph construction,” *arXiv preprint arXiv:1906.05317*, 2019.

[5] T. Brown, B. Mann, N. Ryder, M. Subbiah, J. D. Kaplan, P. Dhariwal, A. Neelakantan, P. Shyam, G. Sastry, A. Askell *et al.*, “Language models are few-shot learners,” *Advances in neural information processing systems*, vol. 33, pp. 1877–1901, 2020.

[6] J. Devlin, M.-W. Chang, K. Lee, and K. Toutanova, “Bert: Pre-training of deep bidirectional transformers for language understanding,” *arXiv preprint arXiv:1810.04805*, 2018.

[7] X. Feng, D. Song, Y. Chen, Z. Chen, J. Ni, and H. Chen, “Convolutional transformer based dual discriminator generative adversarial networks for video anomaly detection,” in *Proceedings of the 29th ACM International Conference on Multimedia*, 2021, pp. 5546–5554.

[8] C. Gao, X. Wang, X. He, and Y. Li, “Graph neural networks for recommender system,” in *Proceedings of the Fifteenth ACM International Conference on Web Search and Data Mining*, 2022, pp. 1623–1625.

[9] D. Gao, K. Li, R. Wang, S. Shan, and X. Chen, “Multi-modal graph neural network for joint reasoning on vision and scene text,” in *Proceedings of the IEEE/CVF conference on computer vision and pattern recognition*, 2020, pp. 12746–12756.

[10] J. Gilmer, S. S. Schoenholz, P. F. Riley, O. Vinyals, and G. E. Dahl, “Neural message passing for quantum chemistry,” in *International conference on machine learning*. PMLR, 2017, pp. 1263–1272.

[11] R. Girdhar, A. El-Nouby, Z. Liu, M. Singh, K. V. Alwala, A. Joulin, and I. Misra, “Imagebind: One embedding space to bind them all,” in *Proceedings of the IEEE/CVF Conference on Computer Vision and Pattern Recognition*, 2023, pp. 15180–15190.

[12] H. Ha, J. Lee, W. Han, and B.-G. Chun, “Meta-learning of prompt generation for lightweight prompt engineering on language-model-as-a-service,” in *The 2023 Conference on Empirical Methods in Natural Language Processing*, 2023.

[13] M. Islam, A. S. Dukyil, S. Alyahya, and S. Habib, “An iot enable anomaly detection system for smart city surveillance,” *Sensors*, vol. 23, no. 4, p. 2358, 2023.

[14] C. Jia, Y. Yang, Y. Xia, Y.-T. Chen, Z. Parekh, H. Pham, Q. Le, Y.-H. Sung, Z. Li, and T. Duerig, “Scaling up visual and vision-language representation learning with noisy text supervision,” in *International conference on machine learning*. PMLR, 2021, pp. 4904–4916.

[15] T. Kojima, S. S. Gu, M. Reid, Y. Matsuo, and Y. Iwasawa, “Large language models are zero-shot reasoners,” *Advances in neural information processing systems*, vol. 35, pp. 22199–22213, 2022.

[16] B. Lester, R. Al-Rfou, and N. Constant, “The power of scale for parameter-efficient prompt tuning,” *arXiv preprint arXiv:2104.08691*, 2021.

[17] G. Li, G. Cai, X. Zeng, and R. Zhao, “Scale-aware spatio-temporal relation learning for video anomaly detection,” in *European Conference on Computer Vision*. Springer, 2022, pp. 333–350.

[18] X. L. Li and P. Liang, “Prefix-tuning: Optimizing continuous prompts for generation,” *arXiv preprint arXiv:2101.00190*, 2021.

[19] W. Liu, D. L. W. Luo, and S. Gao, “Future frame prediction for anomaly detection – a new baseline,” in *2018 IEEE Conference on Computer Vision and Pattern Recognition (CVPR)*, 2018.

[20] Z. Liu, J. Ning, Y. Cao, Y. Wei, Z. Zhang, S. Lin, and H. Hu, “Video swin transformer,” in *Proceedings of the IEEE/CVF conference on computer vision and pattern recognition*, 2022, pp. 3202–3211.

[21] Z. Liu, Y. Nie, C. Long, Q. Zhang, and G. Li, “A hybrid video anomaly detection framework via memory-augmented flow reconstruction and flow-guided frame prediction,” in *Proceedings of the IEEE/CVF international conference on computer vision*, 2021, pp. 13588–13597.

[22] I. Loshchilov and F. Hutter, “Decoupled weight decay regularization,” *arXiv preprint arXiv:1711.05101*, 2017.

[23] H. Lv, C. Chen, Z. Cui, C. Xu, Y. Li, and J. Yang, “Learning normal dynamics in videos with meta prototype network,” in *Proceedings of the IEEE/CVF conference on computer vision and pattern recognition*, 2021, pp. 15425–15434.

[24] S. K. Nanda, D. Ghai, P. Ingole, and S. Pande, “Soft computing techniques-based digital video forensics for fraud medical anomaly detection,” *Computer Assisted Methods in Engineering and Science*, vol. 30, no. 2, pp. 111–130, 2022.

[25] M. G. Narasimhan, “Dynamic video anomaly detection and localization using sparse denoising autoencoders,” *Multimedia Tools and Applications*, vol. 77, pp. 13173–13195, 2018.

[26] J. Pan, S. Chen, M. Z. Shou, Y. Liu, J. Shao, and H. Li, “Actor-context-actor relation network for spatio-temporal action localization,” in *Proceedings of the IEEE/CVF Conference on Computer Vision and Pattern Recognition*, 2021, pp. 464–474.

[27] H. Park, J. Noh, and B. Ham, “Learning memory-guided normality for anomaly detection,” in *Proceedings of the IEEE/CVF conference on computer vision and pattern recognition*, 2020, pp. 14372–14381.

[28] Y. Pu, X. Wu, and S. Wang, “Learning prompt-enhanced context features for weakly-supervised video anomaly detection,” *arXiv preprint arXiv:2306.14451*, 2023.

[29] A. Radford, J. W. Kim, C. Hallacy, A. Ramesh, G. Goh, S. Agarwal, G. Sastry, A. Askell, P. Mishkin, J. Clark *et al.*, “Learning transferable visual models from natural language supervision,” in *International conference on machine learning*. PMLR, 2021, pp. 8748–8763.

[30] K. B. Sahay, B. Balachander, B. Jagadeesh, G. A. Kumar, R. Kumar, and L. R. Parvathy, “A real time crime scene intelligent video surveillance systems in violence detection framework using deep learning techniques,” *Computers and Electrical Engineering*, vol. 103, p. 108319, 2022.

[31] A. Singh, R. Hu, V. Goswami, G. Couairon, W. Galuba, M. Rohrbach, and D. Kiela, “Flava: A foundational language and vision alignment model,” in *Proceedings of the IEEE/CVF Conference on Computer Vision and Pattern Recognition*, 2022, pp. 15638–15650.

[32] L. Song, S. Zhang, G. Yu, and H. Sun, “Taonet: Transition-aware context network for spatio-temporal action detection,” in *Proceedings of the IEEE/CVF Conference on Computer Vision and Pattern Recognition*, 2019, pp. 11987–11995.

[33] D. Sorokin and I. Gurevych, “Modeling semantics with gated graph neural networks for knowledge base question answering,” *arXiv preprint arXiv:1808.04126*, 2018.

[34] R. Speer, J. Chin, and C. Havasi, “Conceptnet 5.5: An open multilingual graph of general knowledge,” in *Proceedings of the AAAI conference on artificial intelligence*, vol. 31, no. 1, 2017.

[35] J. J. P. Suarez and P. C. Naval Jr, “A survey on deep learning techniques for video anomaly detection,” *arXiv preprint arXiv:2009.14146*, 2020.

[36] W. Sultani, C. Chen, and M. Shah, “Real-world anomaly detection in surveillance videos,” in *Proceedings of the IEEE conference on computer vision and pattern recognition*, 2018, pp. 6479–6488.

[37] W. Sultani, C. Chen, and M. Shah, “Real-world anomaly detection in surveillance videos,” in *The IEEE Conference on Computer Vision and Pattern Recognition (CVPR)*, June 2018.

[38] Y. Tian, G. Pang, Y. Chen, R. Singh, J. W. Verjans, and G. Carneiro, “Weakly-supervised video anomaly detection with robust temporal feature magnitude learning,” in *Proceedings of the IEEE/CVF international conference on computer vision*, 2021, pp. 4975–4986.

[39] W. Ullah, T. Hussain, F. U. Min Ullah, K. Muhammad, M. Hassaballah, J. J. Rodrigues, S. W. Baik, and V. H. C. d. Albuquerque, “Ad-graph: Weakly supervised anomaly detection graph neural network,” *International Journal of Intelligent Systems*, vol. 2023, pp. 1–12, 2023.

[40] A. Vaswani, N. Shazeer, N. Parmar, J. Uszkoreit, L. Jones, A. N. Gomez, Ł. Kaiser, and I. Polosukhin, “Attention is all you need,” *Advances in neural information processing systems*, vol. 30, 2017.

[41] P. Veličković, G. Cucurull, A. Casanova, A. Romero, P. Lio, and Y. Bengio, “Graph attention networks,” *arXiv preprint arXiv:1710.10903*, 2017.

[42] G. Wang, X. Yuan, A. Zheng, H.-M. Hsu, and J.-N. Hwang, “Anomaly candidate identification and starting time estimation of vehicles from traffic videos,” in *CVPR workshops*, 2019, pp. 382–390.

[43] M. Wang, J. Xing, and Y. Liu, “Actionclip: A new paradigm for video action recognition,” *arXiv preprint arXiv:2109.08472*, 2021.

[44] M. Wang, J. Xing, J. Mei, Y. Liu, and Y. Jiang, “Actionclip: Adapting language-image pretrained models for video action recognition,” *IEEE Transactions on Neural Networks and Learning Systems*, 2023.

[45] Y. Wang, M. Yasunaga, H. Ren, S. Wada, and J. Leskovec, “Vqa-gnn: Reasoning with multimodal semantic graph for visual question answering,” *arXiv preprint arXiv:2205.11501*, 2022.

[46] B. Workshop, T. L. Scao, A. Fan, C. Akiki, E. Pavlick, S. Ilić, D. Hesslow, R. Castagné, A. S. Luccioni, F. Yvon *et al.*, “Bloom: A 176b-parameter open-access multilingual language model,” *arXiv preprint arXiv:2211.05100*, 2022.

[47] J.-C. Wu, H.-Y. Hsieh, D.-J. Chen, C.-S. Fuh, and T.-L. Liu, “Self-supervised sparse representation for video anomaly detection,” in *European Conference on Computer Vision*. Springer, 2022, pp. 729–745.

[48] P. Wu and J. Liu, “Learning causal temporal relation and feature discrimination for anomaly detection,” *IEEE Transactions on Image Processing*, vol. 30, pp. 3513–3527, 2021.

[49] P. Wu, J. Liu, Y. Shi, Y. Sun, F. Shao, Z. Wu, and Z. Yang, “Not only look, but also listen: Learning multimodal violence detection under weak supervision,” in *European Conference on Computer Vision (ECCV)*, 2020.

[50] H. Xu, G. Ghosh, P.-Y. Huang, D. Okhonko, A. Aghajanyan, F. Metze, L. Zettlemoyer, and C. Feichtenhofer, “Videoclip: Contrastive pre-training for zero-shot video-text understanding,” *arXiv preprint arXiv:2109.14084*, 2021.

[51] M. Yasunaga, H. Ren, A. Bosselut, P. Liang, and J. Leskovec, “Qa-gnn: Reasoning with language models and knowledge graphs for question answering,” *arXiv preprint arXiv:2104.06378*, 2021.

[52] M. Z. Zaheer, A. Mahmood, M. H. Khan, M. Segu, F. Yu, and S.-I. Lee, “Generative cooperative learning for unsupervised video anomaly detection,” in *Proceedings of the IEEE/CVF conference on computer vision and pattern recognition*, 2022, pp. 14 744–14 754.

[53] L. Zanella, B. Liberatori, W. Menapace, F. Poiesi, Y. Wang, and E. Ricci, “Delving into clip latent space for video anomaly recognition,” *arXiv preprint arXiv:2310.02835*, 2023.

[54] G. Zara, S. Roy, P. Rota, and E. Ricci, “Autolabel: Clip-based framework for open-set video domain adaptation,” in *Proceedings of the IEEE/CVF Conference on Computer Vision and Pattern Recognition*, 2023, pp. 11 504–11 513.

[55] J. Zhang, L. Qing, and J. Miao, “Temporal convolutional network with complementary inner bag loss for weakly supervised anomaly detection,” in *2019 IEEE International Conference on Image Processing (ICIP)*. IEEE, 2019, pp. 4030–4034.

[56] S. Zhang, H. Tong, J. Xu, and R. Maciejewski, “Graph convolutional networks: a comprehensive review,” *Computational Social Networks*, vol. 6, no. 1, pp. 1–23, 2019.

[57] J.-X. Zhong, N. Li, W. Kong, S. Liu, T. H. Li, and G. Li, “Graph convolutional label noise cleaner: Train a plug-and-play action classifier for anomaly detection,” in *Proceedings of the IEEE/CVF conference on computer vision and pattern recognition*, 2019, pp. 1237–1246.

[58] K. Zhou, J. Yang, C. C. Loy, and Z. Liu, “Conditional prompt learning for vision-language models,” in *Proceedings of the IEEE/CVF Conference on Computer Vision and Pattern Recognition*, 2022, pp. 16 816–16 825.

[59] K. Zhou, J. Yang, C. C. Loy, and Z. Liu, “Learning to prompt for vision-language models,” *International Journal of Computer Vision*, vol. 130, no. 9, pp. 2337–2348, 2022.

[60] Y. Zhou, Y. Qu, X. Xu, F. Shen, J. Song, and H. Shen, “Batchnorm-based weakly supervised video anomaly detection,” *arXiv preprint arXiv:2311.15367*, 2023.

[61] Y. Zhou, A. I. Muresanu, Z. Han, K. Paster, S. Pitis, H. Chan, and J. Ba, “Large language models are human-level prompt engineers,” *arXiv preprint arXiv:2211.01910*, 2022.